Transportation Research Part C 111 (2020) 616–630

Contents lists available at ScienceDirect

Transportation Research Part C

journal homepage: www.elsevier.com/locate/trc

Scalable traffic stability analysis in mixed-autonomy using continuum models☆

Kuang Huang[a], Xuan Di[b,c,*], Qiang Du[a,c], Xi Chen[d]

[a] Department of Applied Physics and Applied Mathematics, Columbia University, United States
[b] Department of Civil Engineering and Engineering Mechanics, Columbia University, United States
[c] Data Science Institute, Columbia University, United States
[d] Department of Computer Science, Columbia University, United States

ARTICLE INFO

Keywords:
Linear stability analysis
Mean field game
Multi-class continuum models

ABSTRACT

This paper presents scalable traffic stability analysis for both pure connected and autonomous vehicle (CAV) traffic and mixed traffic based on continuum traffic flow models. Human-drive vehicles (HDVs) are modeled by a non-equilibrium traffic flow model, i.e., Aw-Rascle-Zhang (ARZ) to capture HDV traffic's unstable nature. CAVs are modeled by a mean field game describing their non-cooperative behaviors as rational utility-optimizing agents. Working with continuum models helps avoiding scalability issues in microscopic multi-class traffic models. We demonstrate from linear stability analysis that the mean field game traffic flow model behaves differently from traditional traffic flow models and stability can only be proved when the total density is in a certain regime. We also show from numerical experiments that CAVs help stabilize mixed traffic. Further, we quantify the impact of CAV's penetration rate and controller design on traffic stability. The results may provide qualitative insights on traffic stability in mixed-autonomy for human drivers and city planners. The results also provide suggestions on CAV controller design for CAV manufacturers.

1. Introduction

Human-drive vehicle (HDV) traffic is observed to be unstable. Small perturbations caused by driving errors or delays can amplify and develop congestions even from uniform flows (Kerner and Rehborn, 1997). The HDV traffic instability is believed to be caused by human drivers' collective behaviors and leads to less efficient fuel consumption (Cui et al., 2017). With the development of emerging techniques on connected and autonomous vehicles (CAVs) and the increasing number of CAVs prepared to be put on public roads, it is expected that CAVs will help stabilize traffic. A field experiment (Stern et al., 2018) showed that one CAV is able to stabilize the traffic system with approximately twenty vehicles on a ring road. CAVs' capability of stabilizing traffic is also validated using microscopic models for mixed CAV-HDV traffic. In microscopic models, the traffic state is described by vehicles' positions and velocities and the traffic system is described by ordinary differential equations (ODEs).

A microscopic traffic system's stability can be investigated from analytical analysis, simulations or field experiments. For the analytical analysis, linear stability analysis is the most commonly used technique (Wilson and Ward, 2011). Using the linear stability analysis, Jin and Orosz (2014) assumed CAVs to be implemented with Connected Cruise Control (CCC) and analyzed the impact of

☆ This article belongs to the Virtual Special Issue on Mixed Traffic with CAVs.

* Corresponding author at: Department of Civil Engineering and Engineering Mechanics, Columbia University, United States.
E-mail address: sharon.di@columbia.edu (X. Di).

https://doi.org/10.1016/j.trc.2020.01.007
Received 1 June 2019; Received in revised form 30 December 2019; Accepted 9 January 2020
Available online 23 January 2020
0968-090X/

CAVs' connectivity and the CCC controller parameters on the mixed traffic's head-to-tail stability; Cui et al. (2017) analyzed the local stability of the mixed traffic system with one CAV connected to multiple HDVs and discussed the maximum number of HDVs the CAV can stabilize for arbitrary CAV controllers; Wu et al. (2018) analyzed the head-to-tail stability of the mixed traffic system with multiple CAVs and multiple HDVs and quantified the relationship between CAV and HDV numbers to stabilize the traffic; Wang (2018) assumed that CAVs have state delay and time lag and analyzed the head-to-tail stability of the mixed traffic system with one CAV and multiple HDVs to design adaptive and stable CAV controllers; Zhou et al. (2019) introduced a more practical stability criterion that requires subsystem head-to-tail stability and analyzed the mixed traffic system with multiple CAVs and multiple HDVs under the new stability criterion; Gong and Du (2018) assumed CAVs to be implemented with Model Predictive Control (MPC) and established the relationship between the MPC objective function and the MPC control stability of the mixed traffic system with multiple CAVs and multiple HDVs to design stable MPC controllers. Based on simulations, Talebpour and Mahmassani (2016); Yao et al. (2019) implemented the Cooperative Adaptive Cruise Control (CACC) on CAVs and investigated the string stability of the mixed traffic system. Different controller parameters and the CAV's penetration rates are tested to illustrate their relations to the stability. Based on field experiments, Jin and Orosz (2018) implemented CCC on CAVs and tested the head-to-tail stability of the mixed traffic system.

The aforementioned studies on microscopic traffic stability analysis are either restricted to special cases or special types of stability or based on simulations or experiments with limited numbers of vehicles. All of these studies suffer from scalability issues in the sense that they can hardly model the impact of vehicles' topology on stability when there are numerous possible permutations between CAVs and HDVs even if their penetration rates are fixed. One alternative approach to address the scalability issues is the PDE approximation (Barooah et al., 2009; Zheng et al., 2016). This approach suggests to study the stability of continuum traffic flow models which are the limits of microscopic models. The approach is well suited for the mixed traffic since one needs only to concern about the density distributions of different classes.

In continuum traffic flow models, the traffic state is described by the aggregated density and velocity in time and space. The traffic system is then described by partial differential equations (PDEs). For single class traffic, the Lighthill-Whitham-Richards (LWR) model (Lighthill and Whitham, 1955; Richards, 1956) is the most extensively used continuum model, which assumes that the vehicle's speed is directly determined by the local density. To model multi-class traffic flows, the LWR model is extended to multi-class LWR models by proposing multi-class fundamental diagrams (FDs). Different multi-class LWR models distinguish them with each other by the way of computing multi-class speeds and flows. Daganzo (1997); Logghe and Immers (2008) developed multi-class LWR models assuming different classes of vehicles have the same speed. Wong and Wong (2002); Chanut and Buisson (2003); Ngoduy and Liu (2007) developed multi-class LWR models assuming the vehicles' speeds depend on their classes. Levin and Boyles (2016) is one among a few studies that applied multi-class LWR models to the mixed traffic of non-connected autonomous vehicles and human drivers. It proposed a multi-class FD assuming that autonomous vehicles and human drivers have different reaction times. The maximum capacity of the FD varies with the penetration rate of autonomous vehicles. Such a multi-class LWR model is applied to design networked traffic controls in the presence of autonomous vehicles.

Multi-class LWR models are all equilibrium traffic flow models. There are a few studies that developed non-equilibrium models for multi-class traffic (Hoogendoorn and Bovy, 2000; Ngoduy et al., 2009; Ngoduy, 2013a,b; Delis et al., 2018). Those models are derived from gas-kinetic equations (Hoogendoorn and Bovy, 2001) that describe microscopic interactions between vehicles using the generalized density. To the authors' best knowledge, Ngoduy et al. (2009) and its consequent studies (Ngoduy, 2013a,b) are the only literature that analyzed multi-class traffic stability using continuum non-equilibrium models. Ngoduy et al. (2009) modeled dynamics of and interactions between CAVs and HDVs and analyzed the traffic system's stability with respect to the CAV's penetration rate to capture the effect of CAVs on traffic stability.

CAVs' connectivity provides them capability of knowing and reacting to global traffic conditions. Based on such capability, Gong and Du (2018) modeled CAVs' cooperative control using model predictive control (MPC). Wei et al. (2019) designed the CAV's combined steering and longitudinal control using MPC to minimize collision risks. Ghiasi et al. (2019) proposed a CAV control algorithm for speed harmonization. Navas and Milanés (2019) designed an advanced CACC controller that utilizes CAV communications to re- duce inter-vehicle gaps. To test and compare those CAV controllers, one can implement them in simulations. Calvert and van Arem (2020) proposed a generic multi-level framework for doing simulations so that one can easily test different CAV controllers in mixed traffic.

When CAVs do not share a common objective, a non-cooperative game forms. MPC was implemented in Wang et al. (2015) to approximate CAVs' non-cooperative control. However, the MPC solution is generally not an equilibrium of the game. Mean field game is a powerful tool to study such type of games and the mean field solution provides a good approximation to the game's equilibrium (Lasry and Lions, 2007). Chevalier et al., 2015; Huang et al., 2019b; Kachroo et al., 2016; Huang et al., 2019a developed mean field game traffic flow models based on vehicles' velocity control. This paper follows the approach and aims to: (i) build continuum traffic flow models for both pure CAV traffic and mixed CAV-HDV traffic based on mean field games; (ii) analyze traffic stability in both scenarios and quantify the impact of the CAV's penetration rate and the CAV controller design on traffic stability.

The contributions of this paper are as follows:

1. Using the PDE approximation approach, we present scalable mixed traffic stability analysis on continuum traffic flow models.
2. Different from the stability analyses in existing studies, we show that CAVs modeled by some types of mean field games can stabilize traffic in some scenarios even if they are not designed to accomplish such purpose. In other words, the traffic stabilizing effect may originate from CAVs' game-based collective behaviors.
3. Carrying out linear stability analysis, we observe that the proposed mean field game traffic flow model may exhibit both elliptic

and hyperbolic properties in different scenarios, which imposes challenges to stability analysis. We prove that the pure CAV traffic is stable in one scenario.
4. To capture the CAV's stabilizing effect, we propose a coupled system of the unstable ARZ and the mean field game and model an asymmetric interaction between CAVs and HDVs.

The remainder of the paper is organized as follows. Section 2 introduces the modeling assumptions and provides an overview of the necessary modeling tools and concepts. Section 3 formulates models for both pure CAV traffic and mixed CAV-HDV traffic. Based on the proposed models, Section 4 shows the linear stability analysis for pure CAV traffic and Section 5 demonstrates the mixed traffic's stability through numerical experiments.

2. Preliminaries

2.1. Modeling framework and assumptions

This paper aims to model CAVs' connected and intelligent driving behaviors on the macroscopic scale. A majority of studies considered vehicle-to-vehicle (V2V) or vehicle-to-infrastructure (V2I) communications between vehicles. Jin and Orosz (2014); Talebpour and Mahmassani (2016) are the ones among those studies that analyzed the impact of CAVs' connectivity on traffic stability. In this paper we assume a vehicle-to-infrastructure (V2I) communication network for CAVs. Each CAV is capable of knowing the global traffic information from the V2I communication network and there is no communication delay.

Beyond the connectivity, we believe that CAVs' utility-optimizing capability plays an important role in CAVs' stabilizing effect. Wang et al. (2015); Gong et al. (2016) modeled CAVs' such capability by presenting MPC controllers with predefined driving costs for CAVs. However, those studies only solved the MPC on microscopic models with limited numbers of CAVs and the MPC solution is usually not an equilibrium when CAVs are competing with each other. In this paper we assume CAVs are utility-optimizing agents who play a non-cooperative game and solve the game's equilibrium on the macroscopic scale.

Formally we make the following assumptions on the CAV controller:

1. Each CAV observes global CAV and HDV densities on the road.
2. Each CAV controls its speeds to minimize its predefined driving cost on $[0, T]$ and all CAVs have the same form of driving cost.
3. CAVs interact with each other in a non-cooperative way and with HDVs. Each CAV's driving cost depends on global CAV and HDV densities on $[0, T]$.

CAVs satisfying the above assumptions can be considered as agents in a multi-agent system and modeled using a mean field game. In the mean field game, each CAV observes the global traffic conditions at the initial time $t = 0$ and solves the mean field equilibrium on the predefined time horizon $[0, T]$. Then each CAV implements its optimal velocity control solved from the same mean field equilibrium. At the mean field equilibrium, the global traffic density evolution on $[0, T]$ results from all CAVs' optimal velocity controls. No CAV can improve its individual objective by unilaterally switching its velocity control dynamically. Although the CAVs implement their velocity controls in a distributed and non-cooperative way, each CAV's velocity control remains optimal with respect to its own objective function, subject to the equilibrium traffic condition. This paper shall study the traffic stability when CAVs implement their optimal velocity controls at the mean field equilibrium.

Remark 2.1.

- We assume the driving speed as the only control variable of CAVs, which is the same as the LWR model and different from the models based on acceleration controls. However, it will be shown later that CAVs' utility-optimizing capability distinguish CAVs' behaviors from those in the LWR model. The presented mean field game model for CAVs have the forward-backward structure and exhibit both elliptic and hyperbolic properties in different regimes, which is mathematically very different from the LWR model that is a hyperbolic conservation law solved forward.
  Higher order mean field games can be proposed based on acceleration controls but will be hard to analyze both analytically and numerically. CAV traffic models based on acceleration controls will be left for the future research.
- We assume CAVs are homogeneous in the sense that they have the same form of driving cost. This is the assumption used in most existing studies that only distinguish CAVs and HDVs. Only a few studies (Chen et al., 2019) discussed heterogeneity across CAVs in microscopic models. The heterogeneity across CAVs can also be studied under the mean field game framework by assuming different forms of driving costs and proposing multi-class mean field games. But that is out of the scope of this paper.
- The CAVs' planning horizon $[0, T]$ is fixed and predefined according to the traffic scenario. For example, in the numerical experiments we take T to be the total time of traveling two cycles on a ring road with free flow speed. When $T \to 0$, Huang et al., 2019a showed that the mean field game will reduce to an LWR model.
  Based on the same driving cost, one can also formulate a mean field type rolling horizon control with planning time T and an execution time shorter than T. Degond et al. (2014) established the relationship between such a rolling horizon control and the original mean field game.
- Since CAVs are able to observe global traffic densities, CAVs will not have reaction delay.

We need also specify human drivers' behaviors in the mixed CAV-HDV traffic. In this paper we assume that HDVs are not

connected and each HDV determines to accelerate or decelerate based on the local density at its current location. In addition we assume that HDVs cannot distinguish between CAVs and HDVs so HDVs can only observe the total density of CAVs and HDVs. Formally we make the following HDVs' behavioral assumptions:

1. Each HDV only observes local total density.
2. Each HDV controls its acceleration according to the local total density.

Different from microscopic traffic models that study a platoon of vehicles, continuum traffic flow models study the traffic density evolution on a given road whose boundary conditions should be specified. The existence of inflows to and outflows from the road brings mathematical challenges to analyze traffic stability. In this paper we will always assume CAVs and HDVs drive on a closed ring road or an infinitely long highway with no entrance nor exit.

2.2. Mean field game

Mean field game (MFG) is a game-theoretic framework to model complex multi-agent dynamic systems (Lasry and Lions, 2007; Huang et al., 2006). MFG models a large population of homogeneous agents from a continuum level and characterizes their dynamical behaviors through a set of PDEs.

In the MFG framework, a population of N rational utility-optimizing agents are modeled by a dynamic system. The agents interact with each other through their utilities. Assuming that those agents optimize their utilities in a non-cooperative way, a *differential game* is formed.

Exact Nash equilibria to the differential game are generally hard to tackle when N is large. Alternatively, MFG considers the continuum problem as $N \to \infty$. By exploiting the population's density distribution as a mediator to describe the interaction between individuals, MFG assumes that each agent only responds to and contributes to the density distribution. Then the game is decoupled into two procedures and described by two coupled PDEs:

1. A backward Hamilton-Jacobi-Bellman (HJB) equation: Given the density evolution of the population, each agent solves an optimal control problem on a predefined time horizon to obtain a minimal cost. For a generic agent, the optimal control problem can be solved by dynamic programming that derives an HJB equation. The equation is solved backward in time.
2. A forward Fokker-Planck equation: Given individual controls, the population's density evolution resulting from all agents' dynamics is described by a Fokker-Planck equation. The equation is solved forward in time.

Based on our assumptions on CAVs in Section 2.1, we can formulate the CAV traffic as a mean field game on the macroscopic level. On the one hand, the Fokker-Planck equation of the traffic density $\rho(x, t)$ reduces to the continuity equation (CE) that is widely used in continuum traffic flow models. On the other hand, CAVs' optimal speed selections $u(x, t)$ are modeled by the HJB equation. Coupling the two equations we end up with a MFG system on the predefined time horizon $[0, T]$. For general theories and applications of mean field games, see Cardaliaguet (2010).

2.3. Aw-Rascle-Zhang model

The Aw-Rascle-Zhang (ARZ) model (Aw and Rascle, 2000; Aw et al., 2002; Zhang, 2002) is one of the non-equilibrium continuum traffic flow models describing human driving behaviors in terms of acceleration rates. The ARZ model is a second order hyperbolic system with a source term. The system consists of a continuity equation (CE) describing the flow conservation and a momentum equation (ME) prescribing the human driver's dynamic behavior:

$$(CE)\quad \rho_t + (\rho u)_x = 0, \tag{2.1}$$

$$(ME)\quad [u + h(\rho)]_t + u[u + h(\rho)]_x = \frac{1}{\tau}[U(\rho) - u], \tag{2.2}$$

where,

$U(\cdot)$: the desired speed function;
$h(\cdot)$: the hesitation function that is an increasing function of density;
τ: the relaxation time quantifying how fast drivers adapt their current speeds to desired speeds.
The desired speed function $U(\cdot)$ determines the ARZ model's uniform flow solutions $\rho(x, t) \equiv \bar{\rho}$, $u(x, t) \equiv \bar{u} = U(\bar{\rho})$. We shall model HDVs by the ARZ model because of its capability of reproducing human traffic instability near uniform flows (Seibold et al., 2012).

2.4. Traffic stability

In this paper traffic stability refers to a traffic system's stability around uniform flows. In car following models, traffic stability is defined by whether the leading vehicle's disturbance can be dampened by the following vehicle. More concretely, the local stability

refers to stability between consecutive two vehicles while the head-to-tail stability refers to stability from the first vehicle to the last vehicle in a platoon (Zhou et al., 2019). For heterogeneous vehicle platoons, the stability analysis of mixed traffic car following models depends on the topology of vehicles and suffers from scalability issues.

In continuum traffic flow models where the macroscopic traffic density and velocity are modeled, traffic stability is defined by whether the deviations on the density and velocity profile from uniform flows are controlled as time increases. Darbha and Rajagopal (1999) established the mathematical definitions of two types of traffic stability for continuum traffic flow models. Taking the ARZ model as an example. The uniform flows of the ARZ model are described by its constant solutions $\rho(x, t) \equiv \bar{\rho}, u(x, t) \equiv \bar{u} = U(\bar{\rho})$. We have the following definitions of traffic stability:

Definition 2.1. The ARZ model (2.1) (2.2) is stable around the uniform flow $(\bar{\rho}, \bar{u})$ where $\bar{u} = U(\bar{\rho})$ if for any $\varepsilon > 0$, there exists $\delta > 0$ such that for any solution $\rho(x, t)$, $u(x, t)$ to the system:

$$\sup_{0\le t<\infty} \{\|\rho(\cdot,t) - \bar{\rho}\| + \|u(\cdot,t) - \bar{u}\|\} \le \varepsilon, \tag{2.3}$$

whenever

$$\|\rho(\cdot,0) - \bar{\rho}\| + \|u(\cdot,0) - \bar{u}\| \le \delta. \tag{2.4}$$

Here $\|\cdot\|$ is a given norm.

Definition 2.2. The ARZ model (2.1) (2.2) is asymptotically stable around the uniform flow $(\bar{\rho}, \bar{u})$ if it is stable, and:

$$\lim_{t\to\infty} \{\|\rho(\cdot,0) - \bar{\rho}\| + \|u(\cdot,0) - \bar{u}\|\} = 0. \tag{2.5}$$

The asymptotic stability is stronger than Definition 2.1 since the asymptotic stability requires the deviations to disappear as time goes to infinity. When considering small deviations, Definition 2.1 already provides a good characterization of traffic stability. In this paper we will use Definition 2.1 rather than asymptotic stability.

The linear stability is another useful stability concept in analytical analysis. The linear stability is defined as follows:

Definition 2.3. The ARZ model (2.1) (2.2) is linearly stable around the uniform flow $(\bar{\rho}, \bar{u})$ if its linearized system is stable near the zero solution (0, 0).

The linear stability is weaker than Definition 2.1 but easier to analyze for continuum traffic flow models since one only needs to deal with linear PDEs. The ARZ model has a simple linear stability criterion (Seibold et al., 2012):

Theorem 2.1. *The ARZ model (2.1) (2.2) is linearly stable around the uniform flow $(\bar{\rho}, \bar{u})$ where $\bar{u} = U(\bar{\rho})$ if and only if*

$$h'(\bar{\rho}) \ge -U'(\bar{\rho}). \tag{2.6}$$

In the subsequent analysis, we will do the linear stability analysis to the pure CAV traffic model and demonstrate the stability of the mixed CAV-HDV traffic model by numerical experiments. Since CAVs are modeled by a mean field game on a predefined time horizon, the definitions of stability and linear stability should be revised a little, which will be given in the later sections.

3. Model formulation

3.1. Pure CAV traffic: mean field game

Assume that a large population of CAVs are driving on a closed or infinitely long highway without any entrance nor exit. CAVs are designed to control their speeds to minimize their driving costs on the horizon $[0, T]$. An “average" CAV starting from location x_0 at time $t = t_0$ solves the following optimal control problem:

$$V(x_0, t_0) = \min_{v(\cdot)} \int_{t_0}^{T} f(v(t), \rho(x(t), t))dt + V_T(x(T)), \tag{3.1}$$

$$\text{s. t. } \dot{x}(t) = v(t), x(t_0) = x_0, \tag{3.2}$$

where,

$x(\cdot)$: the car's trajectory;
$v(\cdot)$: the car's speed control;
$f(\cdot)$: a given cost function which is assumed to be the same for all CAVs;
$\int_{t_0}^{T} f(v(t), \rho(x(t), t))dt$: the driving cost which is an integral of the cost function along the car's trajectory. It depends on both traffic density and the car's speed;
$V_T(\cdot)$: the terminal cost that represents the car's preference on the final position at time $t = T$.
The optimal cost $V(x, t)$ and optimal velocity field $u(x, t)$ are solved from a set of HJB equations:

$$(HJB)\quad V_t + uV_x + f(u, \rho) = 0, \tag{3.3}$$

$$u = \text{argmin}_{\alpha}\{\alpha V_x + f(\alpha, \rho)\}. \tag{3.4}$$

When all CAVs follow their optimal velocity controls, the system's density evolution is described by the continuity equation:

$$(CE)\ \ \rho_t + (\rho u)_x = 0. \tag{3.5}$$

The mean field game is described by the coupled system (3.3) (3.4) (3.5).

- The initial condition for the forward continuity equation (3.5) is given by the initial density $\rho(x, 0) = \rho_0(x)$.
- The terminal condition for the backward HJB equations (3.3) (3.4) are given by the terminal cost $V(x, T) = V_T(x)$.
- The choice of the spatial boundary condition depends on the traffic scenario. For the closed ring road of fixed length L we specify the periodic boundary condition $\rho(0, t) = \rho(L, t)$, $V(0, t) = V(L, t)$.

Remark 3.1. The terminal cost $V_T(x)$ represents the vehicles' preference on their final positions at time $t = T$ (Lachapelle and Wolfram, 2011). For a ring road or an infinitely long road, all positions are equal and we will set $V_T(x) = C$ where C is any constant. For a finitely long road with an entrance and an exit, we may assume that positions near the exit have smaller terminal costs because vehicles desire to reach the exit before the final time. Discussion on the finitely long road will be left for the future research.

The cost function represents certain driving objective. The choice of the cost function is essential to modeling CAV's driving behavior. In this paper we make the driving objective a combination of the car's kinetic energy, efficiency as well as safety and take the following cost function:

$$f(u, \rho) = \underbrace{\frac{1}{2}\left(\frac{u}{u_{\max}}\right)^2}_{\text{kinetic energy}} - \underbrace{\frac{u}{u_{\max}}}_{\text{efficiency}} + \underbrace{\frac{u\rho}{u_{\max}\rho_{\text{jam}}}}_{\text{safety}}, \tag{3.6}$$

where $u_{\max}$ and ρ_{jam} are the CAV's free flow speed and jam density.

In the cost function (3.6), the first term $\frac{1}{2}(u/u_{\max})^2$ models the car's kinetic energy that is related to the car's energy consumption; the second term $-u/u_{\max}$ models the car's efficiency, minimizing this term means that the car should drive as fast as possible; The last term $u\rho/u_{\max}\rho_{\text{jam}}$ models the driving safety where ρ is the traffic density and u is the car's own speed. This is a penalty term that restricts the car's speed in high density areas. Note that this term does not represent the flow because u is not the aggregated velocity.

The cost function (3.6) is the same as the one proposed in the authors' work (Huang et al., 2019a). The cost function can also be written in a different way:

$$f(u, \rho) = \frac{1}{2u_{\max}^2}(U(\rho) - u)^2 - \frac{1}{2}\left(1 - \frac{\rho}{\rho_{\text{jam}}}\right)^2, \tag{3.7}$$

where $U(\rho)$ is the Greenshields desired speed function:

$$U(\rho) = u_{\max}\left(1 - \frac{\rho}{\rho_{\text{jam}}}\right). \tag{3.8}$$

Eq. (3.7) provides the other way to interpret the cost function (3.6) that CAVs tend to be not too far from human driving as well as to stay in low density areas.

The MFG system corresponding to the cost function (3.6) is:

$$\begin{cases} \rho_t + (\rho u)_x = 0, & \text{(a)} \\ V_t + uV_x + \frac{1}{2}\left(\frac{u}{u_{\max}}\right)^2 - \frac{u}{u_{\max}} + \frac{u\rho}{u_{\max}\rho_{\text{jam}}} = 0, & \text{(b)} \\ u = g_{[0,u_{\max}]}\left(u_{\max}\left(1 - \frac{\rho}{\rho_{\text{jam}}} - u_{\max}V_x\right)\right) & \text{(c)} \end{cases} \tag{3.9}$$

where $g_{[0,u_{\max}]}(u) = \max\{\min\{u, u_{\max}\}, 0\}$ is a cut-off function which ensures the cars' speeds satisfy the constraints $0 \le u \le u_{\max}$. See the authors' work (Huang et al., 2019a) for some theoretical and numerical analysis on the MFG system (3.9a) (3.9b) (3.9c).

The uniform flows of the MFG system (3.9a) (3.9b) (3.9c) are given by

$$\bar{u} = u_{\max}\left(1 - \frac{\bar{\rho}}{\rho_{\text{jam}}}\right), \tag{3.10}$$

which is the same as the Greenshields desired speed function (3.8). Note that Definition 2.1 does not apply to the MFG system since the system is defined and solved on a fixed time horizon $[0, T]$. In this case, we define traffic stability as follows:

Definition 3.1. The MFG system (3.9a) (3.9b) (3.9c) is stable around the uniform flow $(\bar{\rho}, \bar{u})$ where $\bar{u} = u_{max}(1 - \bar{\rho}/\rho_{jam})$ if for any $\varepsilon > 0$, there exists $\delta > 0$ such that for any $T > 0$ and for any solution $\rho^{(T)}(x, t)$, $u^{(T)}(x, t)$ to the system with $V_T(x) = C$ on the time horizon $[0, T]$:

$$\sup_{0\le t\le T}\{||\rho^{(T)}(\cdot,t)-\bar{\rho}||+||u^{(T)}(\cdot,t)-\bar{u}||\}\le\varepsilon, \tag{3.11}$$

whenever

$$||\rho(\cdot,0)-\bar{\rho}||\le\delta. \tag{3.12}$$

The system is linearly stable if its linearized system at $(\bar{\rho},\bar{u})$ is stable around the zero solution.

3.2. Mixed traffic: Coupled MFG-ARZ system

This section aims to develop a continuum mixed CAV-HDV traffic flow model. We denote $\rho^{\mathrm{CAV}}(x,t)$ the CAV density, $\rho^{\mathrm{HDV}}(x,t)$ the HDV density and

$$\rho^{\mathrm{TOT}}(x,t)=\rho^{\mathrm{CAV}}(x,t)+\rho^{\mathrm{HDV}}(x,t), \tag{3.13}$$

the total density. Denote $u^{\mathrm{CAV}}(x,t)$ and $u^{\mathrm{HDV}}(x,t)$ the velocities of CAVs and HDVs, respectively.

Remark 3.2. More general than the total density (3.13), we can define the effective density:

$$\rho^{\mathrm{EFF}}(x,t)=\beta^{\mathrm{CAV}}\rho^{\mathrm{CAV}}(x,t)+\beta^{\mathrm{HDV}}\rho^{\mathrm{HDV}}(x,t), \tag{3.14}$$

where β^{CAV} and β^{HDV} are weights known as the passenger car equivalent (PCE). Logghe and Immers (2003) developed a multi-class LWR model based on the effective density. In this paper we shall use the total density ρ^{TOT} for simplicity.

We model CAVs by the MFG and HDVs by the ARZ model, respectively. The next step is to model the interactions between CAVs and HDVs. Existing studies on multi-class LWR models define multi-class interactions by defining the way of computing and assigning multi-class flows (Logghe and Immers, 2008; Fan and Work, 2015). We shall follow the framework from Work (2015) and model the multi-class flows by the following continuity equations for both CAVs and HDVs:

$$(\mathrm{CE}-\mathrm{CAV})\quad \rho_t^{\mathrm{CAV}}+(\rho^{\mathrm{CAV}}u^{\mathrm{CAV}})_x=0, \tag{3.15}$$

$$(\mathrm{CE}-\mathrm{HDV})\quad \rho_t^{\mathrm{HDV}}+\rho^{\mathrm{HDV}}u^{\mathrm{HDV}}{}_x=0. \tag{3.16}$$

Different from multi-class LWR models, we need also define how CAVs and HDVs influence each other's speed selections when coupling the MFG and ARZ. The CAV's velocity u^{CAV} is solved from the HJB equations of the MFG and the HDV's velocity u^{HDV} is solved from the momentum equation of the ARZ model. So we model the interaction between CAVs and HDVs on speed selections by introducing multi-class densities into the HJB equations and the momentum equation.

Based on the HDVs' behavioral assumption that each HDV only observes local total density, the momentum Eq. (2.2) in the ARZ model becomes:

$$[u^{\mathrm{HDV}}+h(\rho^{\mathrm{TOT}})]_t+u^{\mathrm{HDV}}[u^{\mathrm{HDV}}+h(\rho^{\mathrm{TOT}})]_x=\frac{1}{\tau}[U(\rho^{\mathrm{TOT}})-u^{\mathrm{HDV}}], \tag{3.17}$$

where $U(\rho)$ is chosen to be the Greenshields desired speed function (3.8).

On the other hand, CAVs are assumed to observe both CAV and HDV densities. We model CAVs' reaction to multi-class densities by introducing an extra term into the CAV's cost function. The CAV's modified cost function for mixed traffic is:

$$f(u^{\mathrm{CAV}},\rho^{\mathrm{CAV}},\rho^{\mathrm{HDV}})=\underbrace{\frac{1}{2}\left(\frac{u^{\mathrm{CAV}}}{u_{\max}}\right)^2}_{\text{kinetic energy}}-\underbrace{\frac{u^{\mathrm{CAV}}}{u_{\max}}}_{\text{efficiency}}+\underbrace{\frac{u^{\mathrm{CAV}}\rho^{\mathrm{TOT}}}{u_{\max}\rho_{\mathrm{jam}}}+\beta\frac{\rho^{\mathrm{HDV}}}{\rho_{\mathrm{jam}}}}_{\text{safety}}, \tag{3.18}$$

where the safety is modeled by two penalty terms: one is similar to the penalty term in Eq. (3.6) but the congestion is modeled by the total density ρ^{TOT}, the other quantifies HDV's impact on the CAV's speed selection. The parameter β represents CAV's sensitivity to HDV's density. The HJB equations (3.9b) (3.9c) in the MFG then become:

$$V_t+uV_x+\frac{1}{2}\left(\frac{u^{\mathrm{CAV}}}{u_{\max}}\right)^2-\frac{u^{\mathrm{CAV}}}{u_{\max}}+\frac{u^{\mathrm{CAV}}\rho^{\mathrm{TOT}}}{u_{\max}\rho_{\mathrm{jam}}}+\beta\frac{\rho^{\mathrm{HDV}}}{\rho_{\mathrm{jam}}}=0, \tag{3.19}$$

$$u^{\mathrm{CAV}}=g_{[0,u_{\max}]}\left(u_{\max}\left(1-\frac{\rho^{\mathrm{TOT}}}{\rho_{\mathrm{jam}}}-u_{\max}V_x\right)\right). \tag{3.20}$$

Summarizing all above equations, we have the following coupled MFG-ARZ system:

$$\begin{cases} \rho_t^{\mathrm{CAV}} + (\rho^{\mathrm{CAV}} u^{\mathrm{CAV}})_x = 0, & \text{(a)} \\ V_t + uV_x + \frac{1}{2}\left(\frac{u^{\mathrm{CAV}}}{u_{\max}}\right)^2 - \frac{u^{\mathrm{CAV}}}{u_{\max}} + \frac{u^{\mathrm{CAV}}\rho^{\mathrm{TOT}}}{u_{\max}\rho_{\mathrm{jam}}} + \beta\frac{\rho^{\mathrm{HDV}}}{\rho_{\mathrm{jam}}} = 0, & \text{(b)} \\ u^{\mathrm{CAV}} = g_{[0,u_{\max}]}\left(u_{\max}\left(1 - \frac{\rho^{\mathrm{TOT}}}{\rho_{\mathrm{jam}}} - u_{\max}V_x\right)\right) & \text{(c)} \\ \rho_t^{\mathrm{HDV}} + (\rho^{\mathrm{HDV}} u^{\mathrm{HDV}})_x = 0 & \text{(d)} \\ [u^{\mathrm{HDV}} + h(\rho^{\mathrm{TOT}})]_t + u^{\mathrm{HDV}}[u^{\mathrm{HDV}} + h(\rho^{\mathrm{TOT}})]_x = \frac{1}{\tau}[U(\rho^{\mathrm{TOT}}) - u^{\mathrm{HDV}}] & \text{(e)} \\ \rho^{\mathrm{TOT}} = \rho^{\mathrm{CAV}} + \rho^{\mathrm{HDV}}. & \text{(f)} \end{cases} \tag{3.21}$$

- The initial conditions for the forward continuity equations (3.21a) (3.21d) are given by the initial densities $\rho^{\mathrm{CAV}}(x, 0) = \rho_0^{\mathrm{CAV}}(x)$ and $\rho^{\mathrm{HDV}}(x, 0) = \rho_0^{\mathrm{HDV}}(x)$.
- The initial condition for the momentum Eq. (3.21e) is given by the HDV's initial velocity $u^{\mathrm{HDV}}(x, 0) = u_0^{\mathrm{HDV}}(x)$.
- The terminal condition for the backward HJB Eq. (3.21b) (3.21c) is given by the CAV's terminal cost $V(x, T) = V_T(x)$. We will always set $V_T(x) = C$ where C is any constant.
- We specify the periodic boundary conditions $\rho^{\mathrm{CAV}}(0, t) = \rho^{\mathrm{CAV}}(L, t)$, $\rho^{\mathrm{HDV}}(0, t) = \rho^{\mathrm{HDV}}(L, t)$, $u^{\mathrm{HDV}}(0, t) = u^{\mathrm{HDV}}(L, t)$, $V(0, t) = V(L, t)$.

The uniform flows are defined as the system's constant solutions $\rho^{\mathrm{CAV}}(x, t) \equiv \bar{\rho}^{\mathrm{CAV}}$, $\rho^{\mathrm{HDV}}(x, t) \equiv \bar{\rho}^{\mathrm{HDV}}$,

$$\rho^{\mathrm{TOT}}(x, t) \equiv \bar{\rho}^{\mathrm{TOT}} = \bar{\rho}^{\mathrm{CAV}} + \bar{\rho}^{\mathrm{HDV}}, \tag{3.22}$$

and

$$u^{\mathrm{CAV}}(x, t) \equiv u^{\mathrm{HDV}}(x, t) \equiv \bar{u} = u_{\max}\left(1 - \frac{\bar{\rho}^{\mathrm{TOT}}}{\rho_{\mathrm{jam}}}\right). \tag{3.23}$$

Since CAVs are modeled by a mean field game, the mixed traffic system (3.21a–3.21f) is defined and solved on a predefined time horizon $[0, T]$. Similar to Definition 3.1, traffic stability of the mixed system is defined as follows:

Definition 3.2. The mixed traffic system (3.21a–3.21f) is stable around the uniform flow $(\bar{\rho}^{CAV}, \bar{\rho}^{HDV}, \bar{u})$ which satisfies (3.23) if for any $\varepsilon > 0$, there exists $\delta > 0$ such that for any $T > 0$ and for any solution $\rho^{CAV,(T)}(x, t)$, $u^{CAV,(T)}(x, t)$, $\rho^{HDV,(T)}(x, t)$, $u^{HDV,(T)}(x, t)$ to the system with $V_T(x) = C$ on the time horizon $[0, T]$:

$$\sup_{0\le t\le T}\left\{\sum_{i=\mathrm{CAV,HDV}}[\|\rho^{i,(T)}(\cdot,t) - \bar{\rho}^i\| + \|u^{i,(T)}(\cdot,t) - \bar{u}\|]\right\} \le \varepsilon, \tag{3.24}$$

whenever

$$\sum_{i=\mathrm{CAV,HDV}}\left\|\rho^{i,(T)}(\cdot,0) - \bar{\rho}^i\| + \|u^{\mathrm{HDV},(T)}(\cdot,0) - \bar{u}\right\| \le \delta. \tag{3.25}$$

The system is linearly stable if its linearized system at $(\bar{\rho}^{\mathrm{CAV}}, \bar{\rho}^{\mathrm{HDV}}, \bar{u})$ is stable around the zero solution.

4. Pure CAV Traffic: Linear stability analysis

In this section we will carry out the standard linear stability analysis for the MFG system (3.9a) (3.9b) (3.9c) on a ring road or an infinitely long road.

First simplify the system. By scaling to dimensionless quantities we assume $u_{\max} = 1$ and $\rho_{\mathrm{jam}} = 1$. We remove the speed constraints $0 \le u \le u_{\max}$ since the constraints do not change the system's stability for $0 < \bar{u} < u_{\max}$. The system (3.9a) (3.9b) (3.9c) is then rewritten as:

$$\begin{cases} \rho_t + (\rho u)_x = 0, \\ V_t - \frac{1}{2}u^2 = 0, \\ \rho + u + V_x = 1. \end{cases} \tag{4.1}$$

Eliminating V from the system (4.1) we obtain a new system for the density ρ and velocity u:

$$\begin{cases} \rho_t + (\rho u)_x = 0, \\ u_t + uu_x - (\rho u)_x = 0. \end{cases} \tag{4.2}$$

Suppose the original MFG system (3.9a) (3.9b) (3.9c) has the initial condition $\rho(x, 0) = \rho_0(x)$ and the terminal condition $V(x, T) = 0$. Then the system (4.2) has the same initial condition and the terminal condition $\rho(x, T) + u(x, T) = 1$.

Fix a uniform flow $(\bar{\rho}, \bar{u})$ where $\bar{u} = 1 - \bar{\rho}$. It is a constant solution to the system (4.2) with the initial condition $\rho(x, 0) = \bar{\rho}$ and the terminal condition $\rho(x, T) + u(x, T) = 1$. Suppose we perturb the initial condition a little:

$$\rho(x, 0) = \bar{\rho} + \widetilde{\rho}_0(x), \tag{4.3}$$

and keep the same terminal condition. Denote $\widetilde{\rho}(x, t) = \rho(x, t) - \bar{\rho}$, $\widetilde{u}(x, t) = u(x, t) - \bar{u}$ the consequent perturbation on the solution.

Then we linearize the system (4.2) near the uniform flow $(\bar{\rho}, \bar{u})$ and derive the following linear PDE system for the perturbations $\widetilde{\rho}(x, t)$ and $\widetilde{u}(x, t)$:

$$\begin{cases} \widetilde{\rho}_t + (1 - \bar{\rho})\widetilde{\rho}_x + \bar{\rho}\widetilde{u}_x = 0, \\ \widetilde{u}_t + (\bar{\rho} - 1)\widetilde{\rho}_x + (1 - 2\bar{\rho})\widetilde{u}_x = 0. \end{cases} \tag{4.4}$$

This is also a forward–backward system with the initial condition $\widetilde{\rho}(x, 0) = \widetilde{\rho}_0(x)$ and the terminal condition $\widetilde{\rho}(x, T) + \widetilde{u}(x, T) = 0$. For both ring road and infinitely long road cases we can apply the Fourier analysis to analyze the system's stability. Denote $\hat{\rho}(\xi, t)$ and $\hat{u}(\xi, t)$ the Fourier modes of $\widetilde{\rho}(x, t)$ and $\widetilde{u}(x, t)$, where $\xi = \frac{2\pi k x}{L} (k \in \mathbb{Z})$ for the ring road case or $\xi \in \mathbb{R}$ for the infinitely long road case. For any frequency ξ:

$$\begin{cases} \hat{\rho}_t + i\xi(1 - \bar{\rho})\hat{\rho} + i\xi\bar{\rho}\hat{u} = 0, \\ \hat{u}_t + i\xi(\bar{\rho} - 1)\hat{\rho} + i\xi(1 - 2\bar{\rho})\hat{u} = 0. \end{cases} \tag{4.5}$$

This is an ODE system for $\hat{\rho}(\xi, t)$ and $\hat{u}(\xi, t)$. The initial condition of the system is given by $\hat{\rho}(\xi, 0) = \hat{\rho}_0(\xi)$ where $\hat{\rho}_0(\xi)$ is the Fourier mode of $\widetilde{\rho}_0(x)$ with frequency ξ. The terminal condition is given by $\hat{\rho}(\xi, T) + \hat{u}(\xi, T) = 0$.

The linear PDE system (4.4) is stable near the zero solution under the L^2 norm if and only if there exists a universal constant $C > 0$ such that for any $T > 0$ and ξ, the solution to the ODE system (4.5) on $[0, T]$ satisfies

$$|\hat{\rho}(\xi, t)|^2 + |\hat{u}(\xi, t)|^2 \le C|\hat{\rho}_0(\xi)|^2, \forall\, t \in [0, T]. \tag{4.6}$$

Note that the ODE system (4.5) is homogeneous under the scaling: $\hat{\rho} \to \alpha\hat{\rho}$, $\hat{u} \to \alpha\hat{u}$ for any $\alpha \in \mathbb{R}$. So we can assume $\hat{\rho}_0(\xi) = 1$ without loss of generality. The stability condition then becomes:

$$|\hat{\rho}(\xi, t)|^2 + |\hat{u}(\xi, t)|^2 \le C, \forall\, t \in [0, T]. \tag{4.7}$$

We check the stability condition (4.7) by directly solving the ODE system (4.5) with the initial condition $\hat{\rho}(\xi, 0) = 1$ and the terminal condition $\hat{\rho}(\xi, T) + \hat{u}(\xi, T) = 0$. Denote $r = \sqrt{\bar{\rho}(5\bar{\rho} - 4)}$ and

$$S = \exp\left(-\frac{1}{2}i\xi(-3\bar{\rho} + 2)t\right). \tag{4.8}$$

When $\bar{\rho} \neq \frac{4}{5}$, the solution is:

$$\hat{\rho}(\xi, t) = Se^{-\frac{1}{2}i\xi rt}\frac{(r + \bar{\rho})e^{i\xi rt} + (r - \bar{\rho})e^{i\xi rT}}{r + \bar{\rho} + (r - \bar{\rho})e^{i\xi rT}}, \tag{4.9}$$

$$\hat{u}(\xi, t) = -Se^{-\frac{1}{2}i\xi rt}\frac{(r + 3\bar{\rho} - 2)e^{i\xi rt} + (r - 3\bar{\rho} + 2)e^{i\xi rT}}{r + \bar{\rho} + (r - \bar{\rho})e^{i\xi rT}}. \tag{4.10}$$

When $\bar{\rho} = \frac{4}{5}$, the solution is:

$$\hat{\rho}(\xi, t) = e^{\frac{1}{5}i\xi t}\frac{5i - 2t\xi + 2T\xi}{5i + 2T\xi}, \tag{4.11}$$

$$\hat{u}(\xi, t) = -e^{\frac{1}{5}i\xi t}\frac{5i - t\xi + T\xi}{5i + 2T\xi}. \tag{4.12}$$

$\bar{\rho} = \frac{4}{5}$ is a critical value in the sense that the PDE system (4.4) is elliptic when $0 < \bar{\rho} < \frac{4}{5}$ and hyperbolic when $\frac{4}{5} < \bar{\rho} < 1$. Most traditional traffic flow models such as the LWR model and the ARZ model are purely hyperbolic systems (Lighthill and Whitham, 1955; Seibold et al., 2012) while most well-studied MFGs are purely elliptic (Lasry and Lions, 2007). We observe that the proposed MFG traffic flow model (3.9a) (3.9b) (3.9c) captures both of the two types of behaviors in different scenarios.

In the hyperbolic case we can show the stability from computation:

Theorem 4.1. *For any* $0 < \varepsilon < \frac{1}{5}$, *when* $\frac{4}{5} + \varepsilon < \bar{\rho} < 1$, *the solution* (4.9)(4.10) *satisfies the stability condition* (4.7) *for any* $\xi \in \mathbb{R}$ *with* $C = \frac{7}{2\varepsilon}$.

Proof.. When $\frac{4}{5} + \varepsilon < \bar{\rho} < 1$, we have $r > 0$. Then ξrt and ξrT are real numbers. By direct computation:

$$\left|\hat{\rho}(\xi, t)\right|^2 + |\hat{u}(\xi, t)|^2 = \frac{2[5\bar{\rho}^2 - 5\bar{\rho} + 1 + (\bar{\rho} - 1)\cos(\xi r(t - T))]}{\bar{\rho}[3\bar{\rho} - 2 + 2(\bar{\rho} - 1)\cos(\xi rT)]} \tag{4.13}$$

$$\leq \frac{2[5\bar{\rho}^2 - 5\bar{\rho} + 1 + (1-\bar{\rho})]}{\bar{\rho}\,[3\bar{\rho} - 2 - 2(1-\bar{\rho})]} \tag{4.14}$$

$$= \frac{2(5\bar{\rho}^2 - 6\bar{\rho} + 2)}{\bar{\rho}(5\bar{\rho} - 4)} \tag{4.15}$$

$$\leq \frac{7}{2\varepsilon} \tag{4.16}$$

□

As a corollary, the MFG system (3.9a) (3.9b) (3.9c) is linearly stable near the uniform flow $(\bar{\rho}, \bar{u})$ when $\frac{4}{5} + \varepsilon < \bar{\rho} < 1$ for any $0 < \varepsilon < \frac{1}{5}$ on both a ring road and an infinitely long road. This means the pure CAV traffic is stable when the density is high enough. The stability analysis for the elliptic case when $0 < \bar{\rho} < \frac{4}{5}$ is left for future research.

5. Mixed Traffic: Numerical experiments

In this section we will demonstrate the stability of the system (3.21a–3.21f) for mixed traffic by numerical experiments. We shall run numerical simulations in different scenarios and check the stability in those simulations with an artificial stability criterion. Then we discuss how CAVs' different penetration rates and different controller designs influence the mixed traffic's stability.

5.1. Experimental settings

Take the free flow speed $u_{\max} = 30$ m/s and the jam density $\rho_{\text{jam}} = 1/7.5$ m. In all of the numerical experiments, the length of the ring road $L = 1$ km and the length of the time horizon $T = 2L/u_{\max}$.

Choose the hesitation function $h(\rho)$ in the ARZ model to be:

$$h(\rho) = 9 \text{ m} \Big/ \text{s} \cdot \left(\frac{\rho/\rho_{\text{jam}}}{1 - \rho/\rho_{\text{jam}}}\right)^{1/2}, \tag{5.1}$$

which has the same form as the one used in Seibold et al. (2012). In the ARZ model's source term, choose the desired speed function $U(\rho)$ to be the Greenshields one defined by Eq. (3.8) and the relaxation time to be $\tau = 0.1L/u_{\max}$.

For the coupled MFG-ARZ system (3.21a–3.21f) and its arbitrary uniform flow solution $(\bar{\rho}^{\text{CAV}}, \bar{\rho}^{\text{HDV}}, \bar{u})$, the initial densities are set to be:

$$\rho_0^i(x) = \bar{\rho}^i + 0.1 \times \bar{\rho}^i \sin(2\pi x/L), \tag{5.2}$$

for $i = $ CAV, HDV so that the initial perturbations on both CAV and HDV densities are sine waves whose magnitudes are 10% of the respective uniform densities. The HDV's initial velocity is set to be:

$$u_0^{\text{HDV}}(x) \equiv \bar{u} = u_{\max}\left(1 - \frac{\bar{\rho}^{\text{TOT}}}{\rho_{\text{jam}}}\right), \tag{5.3}$$

where $\bar{\rho}^{\text{TOT}} = \bar{\rho}^{\text{CAV}} + \bar{\rho}^{\text{HDV}}$ so that there is no initial perturbation on the HDV's velocity. The CAV's terminal cost is always set to be $V_T(x) = C$ where C is an arbitrary constant.

Checking the stability conditions (3.24) (3.25) in Definition 3.2 is difficult in numerical simulations because we can not exhaust all possible ε and δ. Alternatively we shall use a simplified stability criterion. Denote $\rho^{\text{CAV},(T)}(x,t)$, $u^{\text{CAV},(T)}(x,t)$, $\rho^{\text{HDV},(T)}(x,t)$, $u^{\text{HDV},(T)}(x,t)$ the solution of the system, for any given norm $\|\cdot\|$, we define an *error function*:

$$E(t) = \sum_{i=\text{CAV,HDV}} [\|\rho^{i,(T)}(\cdot,t) - \bar{\rho}^i\| + \|u^{i,(T)}(\cdot,t) - \bar{u}\|], \tag{5.4}$$

for $0 \leq t \leq T$ and the initial error:

$$E_0 = \sum_{i=\text{CAV,HDV}} \left\|\rho_0^i(\cdot) - \bar{\rho}^i\right\| + \|u_0^{\text{HDV}}(\cdot) - \bar{u}\|. \tag{5.5}$$

The system is said to be unstable if:

$$\sup_{0\leq t\leq T} E(t) \geq 2E_0, \tag{5.6}$$

otherwise it is said to be stable. We will check the stability criterion (5.6) in the numerical experiments using the supremum norm.

5.2. Numerical method

To solve the coupled MFG-ARZ system (3.21a–3.21f) numerically, we apply a finite difference method (FDM). The ring road $[0, L]$ is divided into N_x cells and the time horizon $[0, T]$ is discretized into $N_t + 1$ time steps. Denote Δx and Δt the spatial and temporal mesh size.

We discretize the continuity equations (3.21a) (3.21d) by the Lax-Friedrichs scheme (LeVeque, 1992). We discretize the HJB equations (3.21b) (3.21c) of the MFG by an upwind scheme (Huang et al., 2019a). The momentum equation (3.21e) of the ARZ is transformed into its conservative form (Seibold et al., 2012):

$$y_t + (yu^{\mathrm{HDV}})_x = \frac{1}{\tau}\rho^{\mathrm{HDV}}[U(\rho^{\mathrm{TOT}}) - u^{\mathrm{HDV}}], \tag{5.7}$$

by doing the variable change $y = \rho^{\mathrm{HDV}}[u^{\mathrm{HDV}} + h(\rho^{\mathrm{TOT}})]$. Then we discretize Eq. (5.7) by a hybrid scheme. The hybrid scheme is the combination of the explicit Lax-Friedrichs scheme for the conservation term $(yu^{\mathrm{HDV}})_x$ and the implicit Euler scheme for the relaxation term $\frac{1}{\tau}\rho^{\mathrm{HDV}}[U(\rho^{\mathrm{TOT}}) - u^{\mathrm{HDV}}]$. Denote $(\rho^{\mathrm{CAV}})_j^n$, $(u^{\mathrm{CAV}})_j^n$, $(\rho^{\mathrm{HDV}})_j^n$, $(u^{\mathrm{HDV}})_j^n$, V_j^n and y_j^n the discretization of $\rho^{\mathrm{CAV}}(x, t)$, $u^{\mathrm{CAV}}(x, t)$, $\rho^{\mathrm{HDV}}(x, t)$, $u^{\mathrm{HDV}}(x, t)$, $V(x, t)$ and $y(x, t)$. The coupled MFG-ARZ system (3.21a–3.21f) is discretized as:

$$\begin{cases}
(\rho^{\mathrm{CAV}})_j^{n+1} = \frac{1}{2}[(\rho^{\mathrm{CAV}})_{j-1}^n + (\rho^{\mathrm{CAV}})_{j+1}^n] - \frac{\Delta t}{2\Delta x}[(\rho^{\mathrm{CAV}})_{j+1}^n (u^{\mathrm{CAV}})_{j+1}^n - (\rho^{\mathrm{CAV}})_{j-1}^n (u^{\mathrm{CAV}})_{j-1}^n], & \text{(a)}\\
\frac{V_j^{n+1} - V_j^n}{\Delta t} + (u^{\mathrm{CAV}})_j^n \frac{V_{j+1}^{n+1} - V_j^{n+1}}{\Delta x} + \frac{1}{2}\left(\frac{(u^{\mathrm{CAV}})_j^n}{u_{\max}}\right)^2 - \frac{(u^{\mathrm{CAV}})_j^n}{u_{\max}} + \frac{(u^{\mathrm{CAV}})_j^n (\rho^{\mathrm{TOT}})_j^n}{u_{\max}\rho_{\mathrm{jam}}} \\
\qquad + \beta\frac{(\rho^{\mathrm{HDV}})_j^n}{\rho_{\mathrm{jam}}} = 0, & \text{(b)}\\
(u^{\mathrm{CAV}})_j^n = g_{[0,u_{\max}]}\left(u_{\max}\left(1 - \frac{(\rho^{\mathrm{TOT}})_j^n}{\rho_{\mathrm{jam}}} - u_{\max}\frac{V_{j+1}^{n+1} - V_j^{n+1}}{\Delta x}\right)\right), & \text{(c)}\\
(\rho^{\mathrm{HDV}})_j^{n+1} = \frac{1}{2}[(\rho^{\mathrm{HDV}})_{j-1}^n + (\rho^{\mathrm{HDV}})_{j+1}^n] - \frac{\Delta t}{2\Delta x}[(\rho^{\mathrm{HDV}})_{j+1}^n (u^{\mathrm{HDV}})_{j+1}^n - (\rho^{\mathrm{HDV}})_{j-1}^n (u^{\mathrm{HDV}})_{j-1}^n], & \text{(d)}\\
y_j^{n+\frac{1}{2}} = \frac{1}{2}(y_{j-1}^n + y_{j+1}^n) - \frac{\Delta t}{2\Delta x}[y_{j+1}^n (u^{\mathrm{HDV}})_{j+1}^n - y_{j-1}^n (u^{\mathrm{HDV}})_{j-1}^n], & \text{(e)}\\
y_j^{n+1} = y_j^{n+\frac{1}{2}} + \frac{\Delta t}{\tau}(\rho^{\mathrm{HDV}})_j^{n+1}[U((\rho^{\mathrm{TOT}})_j^{n+1}) - (u^{\mathrm{HDV}})_j^{n+1}], & \text{(f)}\\
(\rho^{\mathrm{TOT}})_j^n = (\rho^{\mathrm{CAV}})_j^n + (\rho^{\mathrm{HDV}})_j^n, & \text{(g)}\\
y_j^n = (\rho^{\mathrm{HDV}})_j^n[(u^{\mathrm{HDV}})_j^n + h((\rho^{\mathrm{TOT}})_j^n)], & \text{(h)}
\end{cases} \tag{5.8}$$

for $j = 1, \ldots, N_x$, $n = 0, \ldots N_t - 1$. The initial and terminal conditions are discretized as:

$$\begin{cases}
(\rho^{\mathrm{CAV}})_j^0 = \frac{1}{\Delta x}\int_{x_{j-1}}^{x_j} \rho_0^{\mathrm{CAV}}(x)dx, & \text{(a)}\\
(\rho^{\mathrm{HDV}})_j^0 = \frac{1}{\Delta x}\int_{x_{j-1}}^{x_j} \rho_0^{\mathrm{HDV}}(x)dx, & \text{(b)}\\
(u^{\mathrm{HDV}})_j^0 = \frac{1}{\Delta x}\int_{x_{j-1}}^{x_j} u_0^{\mathrm{HDV}}(x)dx, & \text{(c)}\\
V_j^{N_t} = V_T(x_j), & \text{(d)}
\end{cases} \tag{5.9}$$

The Eqs. (5.8a–5.8h) together with the initial and terminal conditions (5.9a–5.9d) form a complete system. We solve this nonlinear system by a preconditioned multigrid Newton's method (Huang et al., 2019a).

Using the numerical method, the procedures of numerical experiments are listed in Algorithm 1.

Algorithm 1 Numerical Experiment

Input: Uniform flow $(\bar{\rho}^{\mathrm{CAV}}, \bar{\rho}^{\mathrm{HDV}}, \bar{u})$, parameter β.
output: Whether the mixed traffic is stable or not.

```
Solve ρ^{CAV,(T)}(x, t), u^{CAV,(T)}(x, t), ρ^{HDV,(T)}(x, t) and u^{HDV,(T)}(x, t) from the system (3.21a–3.21f) on [0, T].
Compute the error function E(t) on [0, T] from the solution by Equation (5.4).
if the criterion (5.6) is triggered then
    return unstable
else
    return stable
end if
```

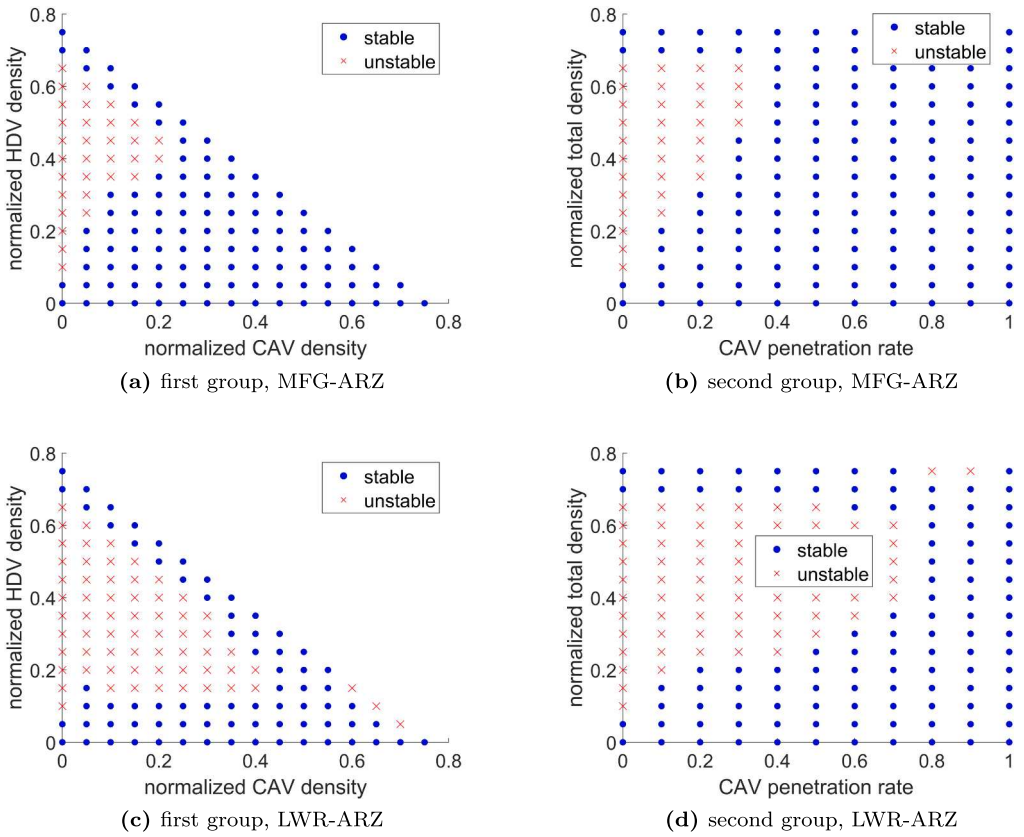

(a) first group, MFG-ARZ (b) second group, MFG-ARZ

(c) first group, LWR-ARZ (d) second group, LWR-ARZ

Fig. 1. Stability regions in the first two groups of numerical experiments for MFG-ARZ and LWR-ARZ.

5.3. Numerical results

In the first group of experiments we fix $\beta = 0$ and try different pairs of values of $\bar{\rho}^{\mathrm{CAV}}$ and $\bar{\rho}^{\mathrm{HDV}}$. We restrict the values to be under $\bar{\rho}^{\mathrm{CAV}} + \bar{\rho}^{\mathrm{HDV}} \leq 0.75\rho_{\mathrm{jam}}$ to avoid the total density exceeding the jam density. We check the system's stability from each numerical experiment and plot the results in the phase diagram between the normalized CAV and HDV density, see Fig. 1(a). We observe that when the HDV density is fixed, adding CAVs makes the traffic more stable. When the CAV density is greater than a critical value determined by the HDV density, the traffic is always stable. When we fix the CAV density and gradually increase the HDV density, we observe that: the traffic is stable when there are a few HDVs, then it becomes unstable in a transition region, finally the traffic is back to stable with a large number of HDVs. When there are only HDVs, the fact that the traffic is stable only for low and high densities is consistent with the ARZ model's stability theory (Seibold et al., 2012) as well as the experimental data from real traffic (Kerner, 1998). The transition region for the HDV density shrinks as the CAV density increases and disappears when the CAV density is equal to or greater than $0.25\rho_{\mathrm{jam}}$. This means the mixed traffic is always stable when the CAV density is large enough.

In the second group of experiments we still keep $\beta = 0$ but try different total densities $\bar{\rho}^{\mathrm{TOT}}$ and different CAV's penetration rates. The total density varies from 0 to $0.75\rho_{\mathrm{jam}}$ and the CAV's penetration rate varies from 0% to 100%. Then we plot the results in the phase diagram between the CAV's penetration rate and the normalized total density, see Fig. 1(b). We observe that when the total density is fixed, traffic becomes more stable with a higher portion of CAVs. In addition, the minimal CAV's penetration rate to stabilize the traffic increases as the total density increases from 0 to $0.7\rho_{\mathrm{jam}}$. When the total density is equal to or larger than $0.7\rho_{\mathrm{jam}}$, the traffic is always stable with any CAV's penetration rate. We also see the unstable transition region of the total density shrinks in Fig. 1(b), which is similar to that of the HDV density in Fig. 1(a). There is a critical CAV's penetration rate 40% such that when the CAV's penetration rate is equal to or greater than such value, traffic is always stable for any total density $0 \leq \bar{\rho}^{\mathrm{TOT}} \leq 0.75\rho_{\mathrm{jam}}$.

Fig. 2 shows a comparison of the total density evolution between a stable example and an unstable example. When the total density is $\bar{\rho}^{\mathrm{TOT}} = 0.4\rho_{\mathrm{jam}}$, the pure HDV traffic is unstable while 30% CAV can stabilize the mixed traffic. Fig. 2(a) shows that in the first case the initial perturbation on the total density amplifies and develops a shock wave with an amplitude more than $0.6\rho_{\mathrm{jam}}$ at the final time; Fig. 2(b) shows that in the second case the initial perturbation decays and the total density converges to a uniform flow at the final time.

The above experiments show that CAVs modeled by the MFG help stabilize traffic. However, it is unclear if the stabilizing effect relates to CAVs' speed control assumption or CAVs' connectivity and utility-optimizing capability. As a comparison, the LWR model which also assumes speed controls but no connectivity nor utility-optimizing capability always produces stable solutions (LeVeque,

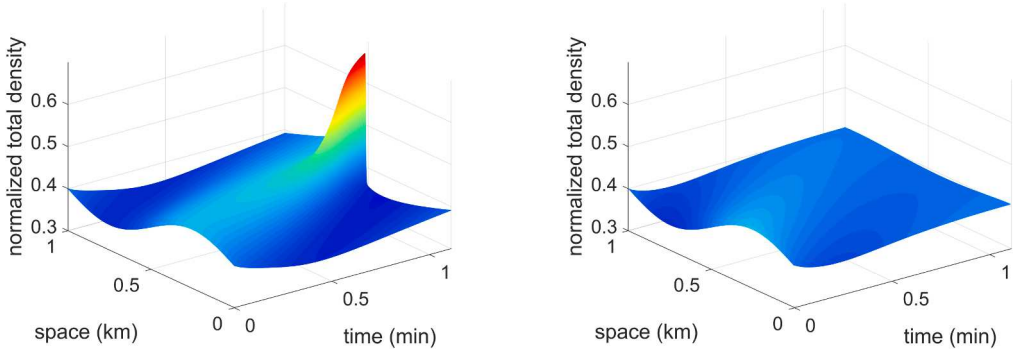

(a) CAV : HDV=0 : 100 **(b)** CAV : HDV=30 : 70

Fig. 2. Comparison of total density evolution with $\beta = 0$, $\bar{\rho}^{\mathrm{TOT}} = 0.4\rho_{\mathrm{jam}}$.

1992). To eliminate the possibility that CAVs' stabilizing effect originates from their speed control assumption, we propose a coupled LWR-ARZ model and compare it with the coupled MFG-ARZ model.

For the coupled LWR-ARZ model, we assume that both CAVs and HDVs only observe local total density. HDVs are modeled by the same ARZ model (3.16) (3.17) while CAVs are modeled by the following LWR model:

$$\rho_t^{\mathrm{CAV}} + (\rho^{\mathrm{CAV}} U(\rho^{\mathrm{TOT}}))_x = 0, \tag{5.10}$$

Then we obtain the coupled LWR-ARZ system (5.10)(3.16)(3.17). In both the LWR model (5.10) and the ARZ model (3.16) (3.17), $U(\rho)$ is chosen as the Greenshields desired speed function defined by Eq. (3.8). Then the coupled LWR-ARZ model's uniform flow solutions are the same as those defined by Eq. (3.23).

The coupled LWR-ARZ system (5.10) (3.16) (3.17) is solved using the Lax-Friedrichs scheme for numerical experiments. We follow the same experimental settings as in Section 5.1 but use a finer mesh to obtain better accuracy without a significant increase in computation. Then we check stability using the same criterion (5.6). We do two groups of experiments and plot the results via two phase diagrams in the same manner as done for the coupled MFG-ARZ model, see Fig. 1(c)(d).

Comparing Fig. 1(c) with Fig. 1(a), we observe that the stability region for the MFG-ARZ is larger than the LWR-ARZ. When the CAV density is equal to or larger than $0.25\rho_{\mathrm{jam}}$, the MFG-ARZ traffic is always stable but the LWR-ARZ traffic is not. Comparing Fig. 1(d) with Fig. 1(b) we see similar patterns. The MFG-ARZ traffic is stable for any total density $0 \le \bar{\rho}^{\mathrm{TOT}} \le 0.75\rho_{\mathrm{jam}}$ whenever CAV's penetration rate is equal to or greater than 40% while the LWR-ARZ traffic is unstable even when the CAV's penetration rate is 70%. The comparison shows that CAVs' connectivity and utility-optimizing capability contribute to CAVs' stabilizing effect.

In the third group of experiments we fix the total density $\bar{\rho}^{\mathrm{TOT}} = 0.5\rho_{\mathrm{jam}}$ and vary the CAV's penetration rate as well as the parameter β. Then we plot the results in the phase diagram between β and the CAV's penetration rate, see Fig. 3. We observe that for any fixed β, increasing the CAV's penetration rate makes the traffic more stable. When the CAV's penetration rate is equal to or greater than 40%, traffic is always stable for any $0 \le \beta \le 1$. On the other hand, if CAVs account for less than 20% of total density, varying β will not stabilize traffic. When the CAV's penetration rate is fixed but equal to or higher than 20%, increasing β makes the traffic more stable. This means that CAVs' stabilizing effect becomes more significant when HDVs have a larger impact on CAVs.

Remark 5.1. We would like to pinpoint that these numerical experiments are not intended to tell exactly what the critical penetration

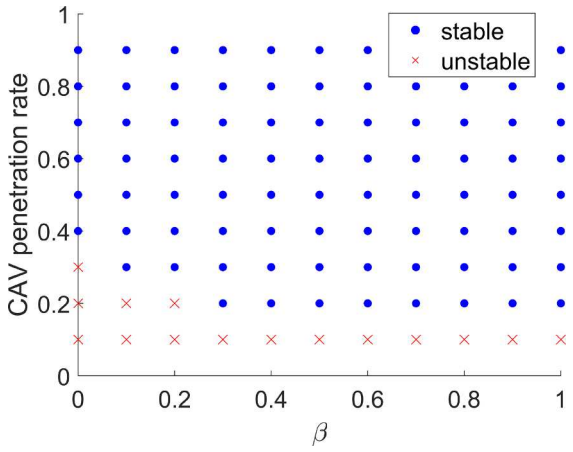

Fig. 3. Stability region for the third group of experiments.

rates of CAVs are to stabilize traffic, which highly depends on CAV and HDV models and the selection of parameters in these models. Instead, we would like to emphasize more on drawing qualitative insights into the trend of possibility as the CAV population grows and how the design of autonomous driving controller may influence traffic stability.

6. Conclusions and future research

This paper presents stability analysis of the mixed traffic composed of both CAVs and HDVs using a continuum multi-class traffic flow model. Unlike multi-class LWR models where CAVs and HDVs only differ in the parameters of fundamental diagrams, the multi-class traffic model developed in this paper assumes two totally distinct driving models for the two types of traffic: the CAV traffic is modeled by a mean field game (MFG), while the HDV traffic is dictated by a non-equilibrium traffic flow model, i.e., the ARZ model.

MFG is a game-theoretic model to capture the dynamic interactions between intelligent agents in a multi-agent environment. Most existing studies simply assumed that CAVs behave like HDVs with shorter reaction time and closer headway. Accordingly, the traffic flow models that are developed for the HDV traffic can be directly applied to model the CAV traffic with parameter modification. But we believe CAVs should be intelligent agents who are utility-optimizing and selecting best-responses considering others' actions. With mean field approximation, the game composed of pure CAVs becomes more tractable to solve. However, the pure CAV traffic may exhibit both elliptic and hyperbolic properties, presenting challenges in stability analysis. Linear stability analysis is performed to demonstrate the stability of the pure CAV traffic when the uniform density is within a regime.

The distinct behavioral features exhibited in CAV and HDV models complicate the coupling between CAV and HDV traffic. We assume both types of vehicles perceive the total traffic density but an asymmetric reaction exists between them. To demonstrate the mixed traffic stability, three groups of numerical experiments are performed. The first two characterize the stability regions over the CAV density and the HDV density as well as over the total density and the CAV's penetration rate in the mixed traffic. We learn that the existence of CAVs could stabilize the mixed traffic and an increasing penetration rate makes the stabilizing effect more significant. We also quantify the impact of the CAV controller parameter on traffic stability: the more sensitively CAVs react to HDVs, the more stable the mixed traffic is.

These conclusions can help transportation engineers and planners to better understand and forecast stability conditions for the mixed CAV-HDV traffic. It could also assist city policy-makers to regulate the design of autonomous driving algorithms with the capability of stabilizing traffic and help CAV manufacturers understand the impacts of different controller parameters on total traffic.

This work still needs to be extended in several ways: (i) Multi-class continuum models provide a more effective and scalable framework for stability analysis of the mixed traffic. However, it is unclear how the macroscopic interactions between two classes of traffic are related to the microscopic interactions between individual vehicles. Understanding such a linkage will offer more insights into why the presence of CAVs could stabilize the mixed traffic. (ii) Only the speed control is employed in the MFG when modeling CAVs' driving behaviors. CAVs' acceleration controls can be modeled by higher order MFGs and will be left for the future research. (iii) CAVs are assumed to be homogeneous in the sense that they have the same cost function and driving parameters. The heterogeneity within the CAV population can be modeled by multi-class MFGs and will be left for future. (iv) In real traffic the road is finitely long and has entrances and exits. Studying continuum traffic models for both the pure CAV traffic and the mixed traffic with the corresponding boundary conditions is one of the future direction.

CRediT authorship contribution statement

Kuang Huang: Methodology, Visualization. **Xuan Di:** Methodology, Writing - review & editing, Supervision. **Qiang Du:** Methodology, Writing - review & editing, Supervision. **Xi Chen:** Supervision.

Acknowledgment

The authors would like to thank Data Science Institute from Columbia University for providing a seed grant for this research.

References

Aw, A., Klar, A., Rascle, M., Materne, T., 2002. Derivation of continuum traffic flow models from microscopic follow-the-leader models. SIAM J. Appl. Math. 63, 259–278.

Aw, A., Rascle, M., 2000. Resurrection of “second order“ models of traffic flow. SIAM J. Appl. Math. 60, 916–938.

Barooah, P., Mehta, P.G., Hespanha, J.P., 2009. Mistuning-based control design to improve closed-loop stability margin of vehicular platoons. IEEE Trans. Autom. Control 54, 2100–2113.

Calvert, S., van Arem, B., 2020... A generic multi-level framework for microscopic traffic simulation with automated vehicles in mixed traffic. Transport. Res. Part C: Emerg. Technol. 110, 291–311.

Cardaliaguet, P., 2010. Notes on mean field games. Technical Report.

Chanut, S., Buisson, C., 2003. Macroscopic model and its numerical solution for two-flow mixed traffic with different speeds and lengths. Transp. Res. Rec. 1852, 209–219.

Chen, D., Srivastava, A., Ahn, S., Li, T., 2019. Traffic dynamics under speed disturbance in mixed traffic with automated and non-automated vehicles. Transport. Res. Part C: Emerg. Technol.

Chevalier, G., Le Ny, J., Malhamé, R., 2015. A micro-macro traffic model based on mean-field games. In: 2015 American Control Conference (ACC). IEEE, pp. 1983–1988.

Cui, S., Seibold, B., Stern, R., Work, D.B., 2017. Stabilizing traffic flow via a single autonomous vehicle: Possibilities and limitations. In: 2017 IEEE Intelligent Vehicles Symposium (IV). IEEE, pp. 1336–1341.

Daganzo, C.F., 1997. A continuum theory of traffic dynamics for freeways with special lanes. Transport. Res. Part B: Methodol. 31, 83–102.
Darbha, S., Rajagopal, K., 1999. Intelligent cruise control systems and traffic flow stability. Transport. Res. Part C: Emerg. Technol. 7, 329–352.
Degond, P., Herty, M., Liu, J.G., 2014. Mean field games and model predictive control. arXiv preprint arXiv:1412.7517.
Delis, A.I., Nikolos, I.K., Papageorgiou, M., 2018. A macroscopic multi-lane traffic flow model for ACC/CACC traffic dynamics. Transp. Res. Rec. 2672, 178–192.
Fan, S., Work, D.B., 2015. A heterogeneous multiclass traffic flow model with creeping. SIAM J. Appl. Math. 75, 813–835.
Ghiasi, A., Li, X., Ma, J., 2019. A mixed traffic speed harmonization model with connected autonomous vehicles. Transport. Res. Part C: Emerg. Technol. 104, 210–233.
Gong, S., Du, L., 2018. Cooperative platoon control for a mixed traffic flow including human drive vehicles and connected and autonomous vehicles. Transport. Res. Part B: Methodol. 116, 25–61.
Gong, S., Shen, J., Du, L., 2016. Constrained optimization and distributed computation based car following control of a connected and autonomous vehicle platoon. Transport. Res. Part B: Methodol. 94, 314–334.
Hoogendoorn, S.P., Bovy, P.H., 2000. Continuum modeling of multiclass traffic flow. Transport. Res. Part B: Methodol. 34, 123–146.
Hoogendoorn, S.P., Bovy, P.H., 2001. Generic gas-kinetic traffic systems modeling with applications to vehicular traffic flow. Transport. Res. Part B: Methodol. 35, 317–336.
Huang, K., Di, X., Du, Q., Chen, X., 2019a. A Game-Theoretic Framework for Autonomous Vehicles Velocity Control: Bridging Microscopic Differential Games and Macroscopic Mean Field Games. Submitted to Discrete and Continuous Dynamical Systems - Series B (passed the 1st round review), available at arXiv: 1903.06053.
Huang, K., Di, X., Du, Q., Chen, X., 2019b. Stabilizing traffic via autonomous vehicles: a continuum mean field game approach. In: The 22nd IEEE International Conference on Intelligent Transportation Systems (ITSC), https://doi.org/10.1109/ITSC.2019.8917021.
Huang, M., Malhamé, R.P., Caines, P.E., et al., 2006. Large population stochastic dynamic games: closed-loop Mckean-Vlasov systems and the Nash certainty equivalence principle. Commun. Informat. Syst. 6, 221–252.
Jin, I.G., Orosz, G., 2014. Dynamics of connected vehicle systems with delayed acceleration feedback. Transport. Res. Part C: Emerg. Technol. 46, 46–64.
Jin, I.G., Orosz, G., 2018. Connected cruise control among human-driven vehicles: Experiment-based parameter estimation and optimal control design. Transport. Res. Part C: Emerg. Technol. 95, 445–459.
Kachroo, P., Agarwal, S., Sastry, S., 2016. Inverse problem for non-viscous mean field control: Example from traffic. IEEE Trans. Autom. Control 61, 3412–3421.
Kerner, B.S., 1998. Experimental features of self-organization in traffic flow. Phys. Rev. Lett. 81, 3797.
Kerner, B.S., Rehborn, H., 1997. Experimental properties of phase transitions in traffic flow. Phys. Rev. Lett. 79, 4030.
Lachapelle, A., Wolfram, M.T., 2011. On a mean field game approach modeling congestion and aversion in pedestrian crowds. Transport. Res. Part B: Methodol. 45, 1572–1589.
Lasry, J.M., Lions, P.L., 2007. Mean field games. Japan. J. Math. 2, 229–260.
LeVeque, R.J., 1992. Numerical Methods for Conservation Laws. Springer.
Levin, M.W., Boyles, S.D., 2016. A multiclass cell transmission model for shared human and autonomous vehicle roads. Transport. Res. Part C: Emerg. Technol. 62, 103–116.
Lighthill, M.J., Whitham, G.B., 1955. On kinematic waves II. A theory of traffic flow on long crowded roads. Proc. R. Soc. Lond. A 229, 317–345.
Logghe, S., Immers, L., 2003. Heterogeneous traffic flow modelling with the LWR model using passenger-car equivalents. Proceedings of the 10th World congress on ITS, Madrid (Spain).
Logghe, S., Immers, L.H., 2008. Multi-class kinematic wave theory of traffic flow. Transportat. Res. Part B: Methodol. 42, 523–541.
Navas, F., Milanés, V., 2019. Mixing V2V-and non-V2V-equipped vehicles in car following. Transport. Res. Part C: Emerg. Technol. 108, 167–181.
Ngoduy, D., 2013a. Analytical studies on the instabilities of heterogeneous intelligent traffic flow. Commun. Nonlinear Sci. Numer. Simul. 18, 2699–2706.
Ngoduy, D., 2013b. Instability of cooperative adaptive cruise control traffic flow: A macroscopic approach. Commun. Nonlinear Sci. Numer. Simul. 18, 2838–2851.
Ngoduy, D., Hoogendoorn, S., Liu, R., 2009. Continuum modeling of cooperative traffic flow dynamics. Physica A 388, 2705–2716.
Ngoduy, D., Liu, R., 2007. Multiclass first-order simulation model to explain non-linear traffic phenomena. Physica A 385, 667–682.
Richards, P.I., 1956. Shock waves on the highway. Oper. Res. 4, 42–51.
Seibold, B., Flynn, M.R., Kasimov, A.R., Rosales, R.R., 2012. Constructing set-valued fundamental diagrams from jamiton solutions in second order traffic models . arXiv preprint arXiv:1204.5510.
Stern, R.E., Cui, S., Delle Monache, M.L., Bhadani, R., Bunting, M., Churchill, M., Hamilton, N., Pohlmann, H., Wu, F., Piccoli, B., et al., 2018. Dissipation of stop-and-go waves via control of autonomous vehicles: Field experiments. Transport. Res. Part C: Emerg. Technol. 89, 205–221.
Talebpour, A., Mahmassani, H.S., 2016. Influence of connected and autonomous vehicles on traffic flow stability and throughput. Transport. Res. Part C: Emerg. Technol. 71, 143–163.
Wang, M., 2018. Infrastructure assisted adaptive driving to stabilise heterogeneous vehicle strings. Transport. Res. Part C: Emerg. Technol. 91, 276–295.
Wang, M., Hoogendoorn, S.P., Daamen, W., van Arem, B., Happee, R., 2015. Game theoretic approach for predictive lane-changing and car-following control. Transport. Res. Part C: Emerg. Technol. 58, 73–92.
Wei, C., Romano, R., Merat, N., Wang, Y., Hu, C., Taghavifar, H., Hajiseyedjavadi, F., Boer, E.R., 2019. Risk-based autonomous vehicle motion control with considering human driver's behaviour. Transport. Res. Part C: Emerg. Technol. 107, 1–14.
Wilson, R.E., Ward, J.A., 2011. Car-following models: fifty years of linear stability analysis–a mathematical perspective. Transport. Plann. Technol. 34, 3–18.
Wong, G., Wong, S., 2002. A multi-class traffic flow model–an extension of LWR model with heterogeneous drivers. Transport. Res. Part A: Policy Practice 36, 827–841.
Wu, C., Bayen, A.M., Mehta, A., 2018. Stabilizing traffic with autonomous vehicles. In: 2018 IEEE International Conference on Robotics and Automation (ICRA). IEEE, pp. 1–7.
Yao, Z., Hu, R., Wang, Y., Jiang, Y., Ran, B., Chen, Y., 2019. Stability analysis and the fundamental diagram for mixed connected automated and human-driven vehicles. Physica A 533, 121931.
Zhang, H.M., 2002. A non-equilibrium traffic model devoid of gas-like behavior. Transport. Res. Part B: Methodol. 36, 275–290.
Zheng, Y., Li, S.E., Li, K., Wang, L.Y., 2016. Stability margin improvement of vehicular platoon considering undirected topology and asymmetric control. IEEE Trans. Control Syst. Technol. 24, 1253–1265.
Zhou, Y., Ahn, S., Wang, M., Hoogendoorn, S., 2019. Stabilizing mixed vehicular platoons with connected automated vehicles: An H-infinity approach. Transport. Res. Part B: Methodol.